Fracture Mechanics of Concrete Structures
Proceedings FRAMCOS-3
AEDIFICATIO Publishers, D-79104 Freiburg, Germany

FRACTURE PROPERTIES OF HIGH STRENGTH CONCRETE

X. Yin
KPFF Engineers, Portland, OR, USA
J. Stanton
Department of Civil Engineering, University of Washington, Seattle, USA
N. Hawkins
Department of Civil Engineering, University of Illinois at Urbana-Champaign, USA

Abstract

CLWL-DCB specimens were used to study the fracture properties of normal and high strength normalweight concretes and of high strength lightweight aggregate concretes. A three segment fracture process zone model developed in prior studies, when modified appropriately, predicted well the relative fracture behavior of the three concretes. Modifications to differentiate between mixes were necessary primarily in the final segment of the model where the crack closing stress decreased slowly to zero with increasing crack widths. The fracture energy provided by that segment for a 112 MPa dense aggregate concrete was only about half that for a 28 MPa dense aggregate concrete. For a 79 MPa lightweight aggregate concrete the fracture energy provided by that segment was less than 10 % of that for the 28 MPa dense aggregate concrete. There was a clear correlation between the smoothness of the fracture surface and the fracture energy of that final segment.
Key words: Fracture process zone, concretes: high strength and lightweight

1 Introduction

The work described in this paper is the final stage of an investigation conducted at the University of Washington into the fracture properties of concrete. In prior phases extensive testing of dense aggregate normal strength concretes was conducted using crack line wedge loaded-double cantilever beam (CLWL-DCB) specimens subjected to Mode I loading. The material parameters included in the data base were concrete compressive strength, specimen size, and maximum coarse aggregate size. From the experimental results a non linear model for the fracture process zone (FPZ) that exists behind the crack tip was developed through the interactive use of the experimental data and finite element analysis. Relevant prior experimental data is summarized in Jeang and Hawkins (1985) and the nonlinear model for fracture developed from that data is described in Liaw et al. (1990).

In this investigation displacement controlled fracture tests were made on CLWL-DCB specimens containing silica fume and both light and normal weight aggregates. Based on those results the non linear finite element model developed previously was extended to cover light and normal weight high strength concretes. Comprehensive details of the test program, test results and the development of the finite element models are provided in Yin (1997).

2 Test Program

Tests were conducted on 17 CLWL-DCB specimens having the characteristics summarized in Table 1. Three series of specimens B, C and

Table 1. Characteristics of test specimens

Series	No. of Specimens Tested	Size, W inch	f'_c (Age) psi (days)	Concrete Type (1)	Fine Aggregate Type (2)	Coarse Aggregate Type (3)	inch
B 1	1	15	3,940 (80)	N	D	N	1/4
B 2	3	15	4,130 (75)	N	D	N	1/4
C 1	3	15	15,950 (237)	SF	D	N	1/4
C 2	2	15	15,940 (130)	SF	U	N	1/4
C 3	2	15	16,660 (132)	SF	U	N	1/4
D 1	2	22.5	11,320 (128)	SF	D	L	3/4
D 2	2	15	12,200 (116)	SF	U	L	1/4
D 3	2	15	10,700 (113)	SF	U	L	1/4

1 inch = 25.4 mm 1,000 psi = 6.895 Mpa

(1) Concrete: N: normal; SF: silica fume (2) Gradation: U: uniform; D:as delivered

(3) Aggregate type: N: gravel; L: lightweight

D were tested. Series B were normal strength dense aggregate concrete specimens and the sand for the mix was used in its as delivered condition. Series C and D were high strength concrete specimens made with dense and light weight aggregates, respectively. The sand for those mixes was sieved and then recombined to provide a uniform gradation. In general identical pairs of specimens were tested with properties varied between pairs.

The geometry of a typical test specimen is shown in Fig. 1. Most specimens had a characteristic dimension W of 381mm and a thickness of 51 mm. However, for series D1 all dimensions, except for the 76 mm loading hole, were 50% greater than the dimensions shown on Fig. 1. The age of the specimens at test varied as shown in Table 1. Concrete strengths at test averaged 27.8 MPa for the normal strength dense aggregate concrete and 111.6 and 78.6 MPa for the high strength dense and lightweight aggregate concretes, respectively. The maximum size of the aggregate was 6 mm except for the larger specimens for which that size was 19 mm. Appropriate procedures for casting silica fume concretes using either dense or lightweight aggregates were developed in a series of preliminary tests. The cement used was Type 1 with a C_3A content less than 8%. The condensed silica fume and superplasticizer M-150 were supplied by Norcem Concrete Products and the lightweight aggregates were provided by Solite Corporation. Sand and gravel for the mixes were purchased locally. A typical mix contained 0.45 kg of cement, 0.41 kg of sand, 0.73 kg of gravel or 0.43 kg of Solite, 0.09 kg of silica fume and 15,000 ml of M-150.

Care was taken to maintain constant moisture conditions for the aggregates

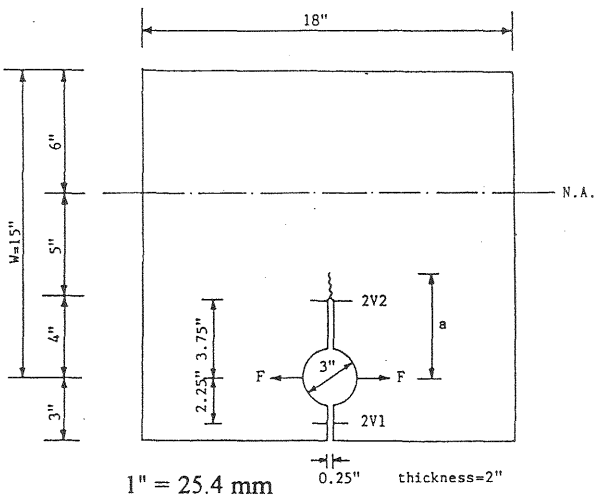

Fig. 1 Geometry of typical test specimen

prior to mixing and for the specimens after casting. Coarse aggregates were stored in sealed metal drums and fine aggregates, as well as the silica fume, were kept in sealed plastic bags. Specimens and control cylinders were removed from the steel molds, in which they were cast, one day after manufacture and placed in a moist room at 100% humidity. At two weeks specimens were briefly removed from the moist room and their upper surface polished. The specimen was then immediately returned to the moist room and not removed again until tested.

The typical specimen had a 178 mm long, 6 mm wide, crack cast into one side and a 76 mm diameter hole located 76 mm from one edge. Specimens were loaded using a wedge inserted through a split pin placed in the 76 mm diameter hole. Load cells within the pin measured the force F applied laterally by the wedge to the specimen. Details of the development of that wedge and split pin loading system are described in Akutagawa (1984). Changes in crack width were measured at two locations, $2V_1$ and $2V_2$, at either end of the precast notch using clip gages. The length of the crack on the polished surface of the specimen was recorded using a replica film technique. That technique was also used to examine the surface prior to the start of testing to ensure that no shrinkage crack had developed from the tip of the precast notch. When such a crack was detected the specimen was discarded.

A typical load history- time relationship is shown in Fig. 2. The wedge was displaced at a rate of 0.15 mm/minute and the load F, and the CODs $2V_1$ and $2V_2$, recorded continuously. When the load reached its peak value the displacement was held constant for about 5 minutes and total crack length "a"

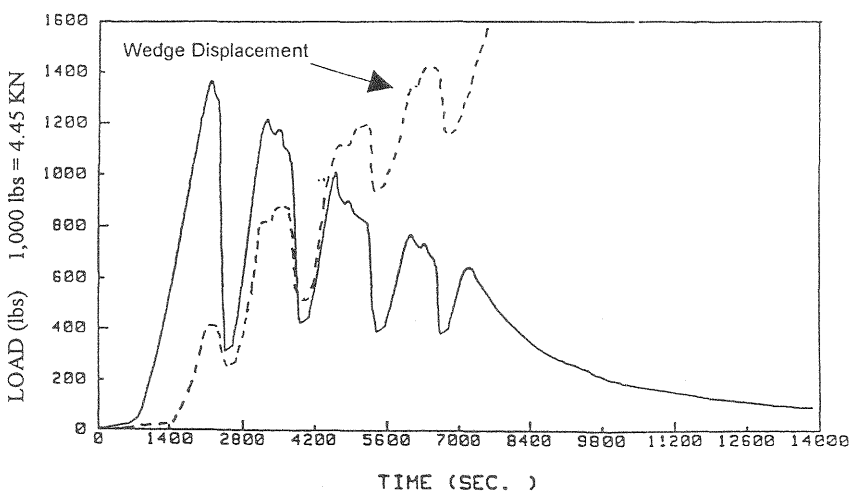

Fig. 2 Typical load-time relationship - specimen B1

measured using a replica film. A partial unload-reload cycle was then applied and the traction free crack length determined from the compliance. Increasing displacement of the wedge was then resumed using the same loading rate and with periodic breaks to measure crack length and unload-reload cycles to measure compliances. Displacements were increased until the load had dropped to less than 0.2 KN. For specimen B1, for example, five crack length measurements were made between peak load and the end of testing.

3 Test Results

Load F-$2V_1$ and load F-a/W relationships for specimens from the three test mixes, B, C and D are shown in Figs. 3, 4 and 5, respectively. Data points obtained during the tests are indicated by symbols. Curves, with symbols attached, indicate results computed using the crack closing stress-crack opening displacement (CCS-COD) model described later.

For the F-$2V_1$ relationships and dense aggregate concretes the peak load for the 111.6 MPa concrete was more than double that for the 27.8 MPa concrete. However, for the high strength lightweight aggregate concrete the peak load was only one third greater than that for the 27.8 MPa concrete even though its compressive strength was almost three times greater. Relative peak load values for all three concretes were consistent with their relative tensile strengths as established from direct tension tests. Yet by a $2V_1$ value of 0.3 mm the load that could be carried for all three mixes was essentially the same.

For the F-a/W relationships for all three mixes the quantity a is the crack length shown on Fig. 1 and values were determined from the replica films.

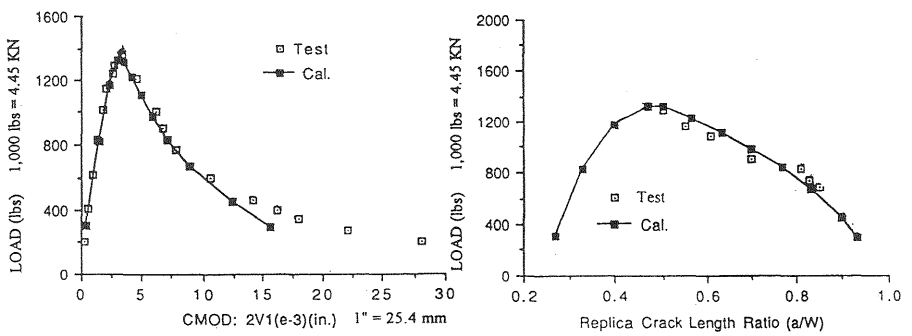

Fig. 3 Load-$2V_1$ and load-a/W relationships for specimen B1

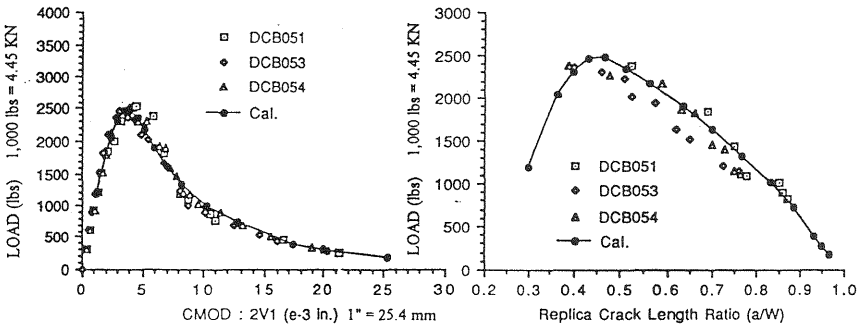

Fig. 4. Load-$2V_1$ and load-a/W relationships for Series C1

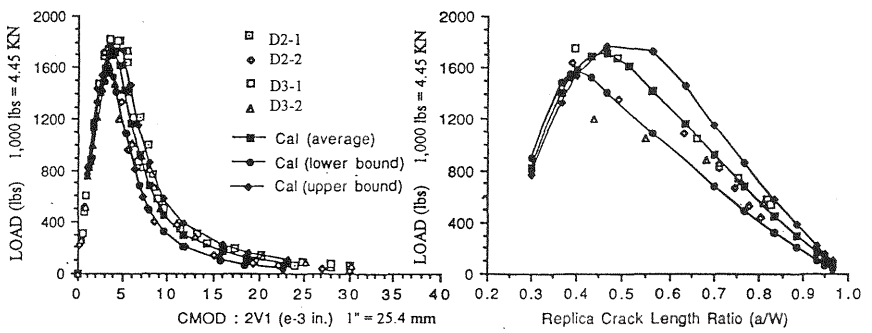

Fig. 5. Load-$2V_1$ and load-a/W relationships for series D2 and D3

W was the characteristic dimension of the DCB specimen and equal to 381 and 572 mm for the small and large specimens, respectively. Peak loads were typically achieved at a/W values of 0.5 for the low strength, and 0.45 for the high strength, dense aggregate concretes and at 0.35 for the high strength lightweight aggregate concrete. Crack extension prior to peak load decreased with increasing brittleness of the concrete and was least for the high strength lightweight aggregate concrete. Variations in the post-peak load capacity with increasing a/W values followed the same trend with load for a given a/W decreasing with increasing brittleness of the concrete.

Crack trajectories for the top and bottom surfaces of typical specimens are shown in Fig. 6. For the 27.8 MPa dense aggregate concrete there was little branching at the crack tip which passed around the coarse aggregate particles and through the concrete matrix, resulting in a fracture surface that was noticeably rough. There was also a general tortuosity with the crack location

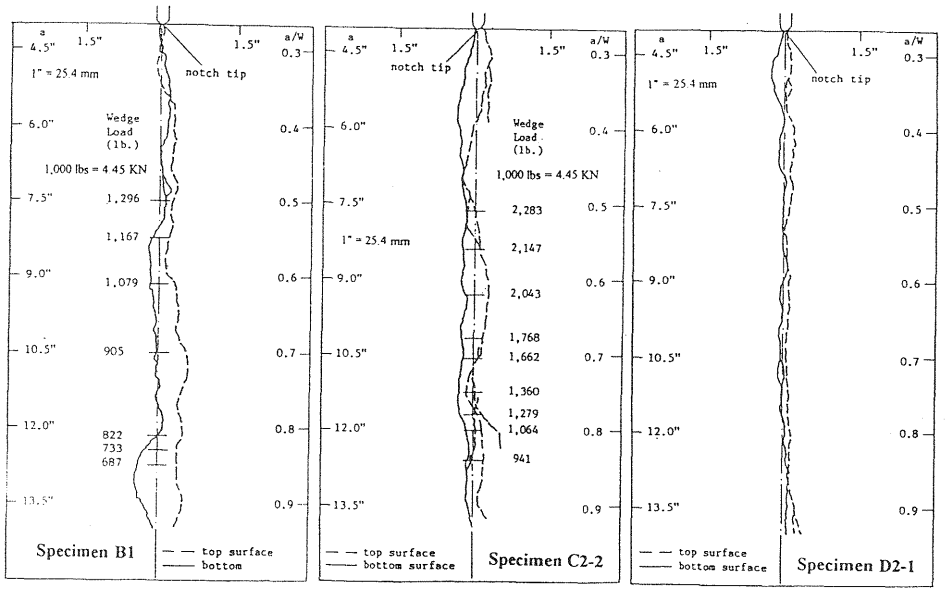

Fig. 6. Typical crack trajectories

on one side of the specimen differing from that on the other. For duplicate specimens the post peak load for a given $2V_1$ value increased as the tortuosity increased. For the silica fume concretes several micro cracks formed around the crack tip making that tip less defined and more difficult to detect. For the lightweight aggregate concrete the crack profiles on the upper and lower surfaces almost coincided. For the dense aggregate 111.6 MPa concrete those profiles differed by about the same amount as for the 27.8 MPa concrete. However, for the 111.6 MPa concrete there was much more crack branching that was visible even after the load was removed. For the lightweight concrete the crack ran directly through the aggregate resulting in a smooth crack surface. For the 111.6 MPa dense aggregate concrete the crack often propagated around the coarse aggregate particles. A count showed that only 70% of the coarse aggregate particles in a typical crack path had fractured. Thus, the fracture surface was smoother, but the tortuosity almost the same, as for the 27.8 MPa dense aggregate concrete.

4 Numerical analysis of results

In prior studies of dense aggregate concretes with strengths varying between

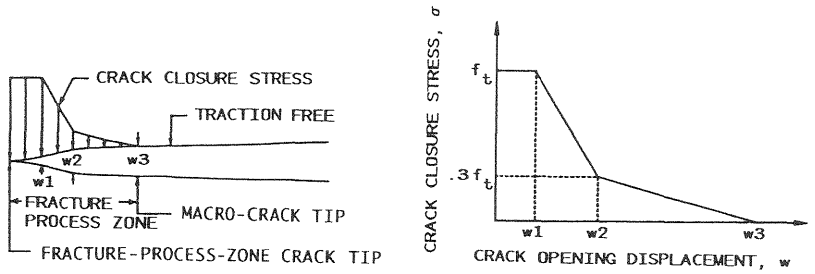

For $3{,}470 \le f'_c \le 5{,}010$ psi ($23.5 \le f'_c \le 34.6$ MPA)

$$w_1 = \left(\frac{0.10f'_c}{1{,}000} - 0.10\right) \times 10^{-3} \text{ in.}$$

$$w_2 = \left(\frac{0.50f'_c}{1{,}000} - 0.50\right) \times 10^{-3} \text{ in.} = 5w_1$$

$$w_3 = w_1 + 9.0 \times 10^{-3} \text{ in}$$

Fig. 7 Fracture process zone model

23.5 and 62.6 MPa Liaw et al. (1990) found through the use of a hybrid experimental-numerical technique that the best agreement between measured and computed results was obtained with an FPZ model that related the CCS to the COD as shown in Fig. 7. Each of the three segments of Fig. 7 were necessary to explain the global results for specimens of differing sizes, loading histories and concrete strengths. For CODs less than w_1 a zone of plasticity with the CCS equal to the tensile strength of the concrete was necessary. Microscopically, that plateau implies a region of discontinuous cracking due to actual cracking, branching or shielding of the main crack tip by surrounding matrix shrinkage cracks. In the second zone the CCS decreased rapidly with increasing COD. The characteristics of this zone are determined by the cracking characteristics of the cement matrix and the aggregate to paste interface. In the third zone the CCS decreased slowly with increasing COD. This zone is necessary for accurate predictions of specimen size effects. The characteristics of this zone are determined by the ability of the aggregate to bridge across the crack. Shown in Fig. 7 are the values of w_1, w_2 and w_3 found appropriate for dense aggregate mixes with uniformly graded sand, coarse aggregate between 6 and 19 mm in maximum size and concrete strengths ranging between 23.5 and 34.6 MPa.

Shown in Fig.8 are the CCS-COD relationships derived from the test data for the mixes reported here. The vertical axis is non-dimensionalized by dividing the CCS value by the tensile strength of the concrete as determined from direct tension tests on samples cut from the DCB specimens after the

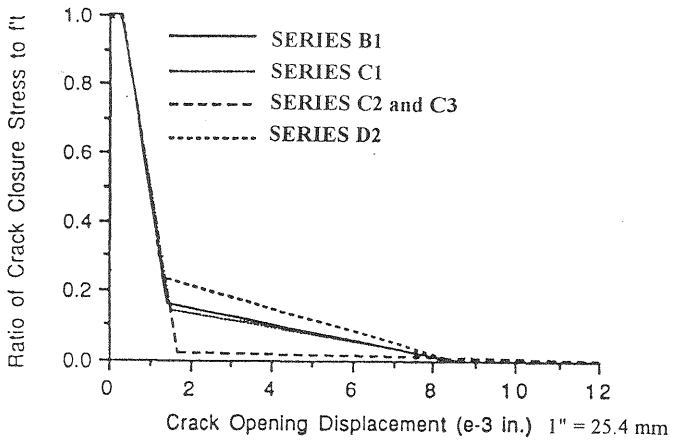

Fig. 8. Optimized FPZ models

fracture tests were completed. Curve B1 is for a dense aggregate concretewith a strength of 27.6 MPa and its use gives good agreement with the results for mix B. Curves C1 and C2 are for high strength dense aggregate concrete with the differences in the curves reflecting the adjustment necessary to account for the effect of a uniform versus as delivered sand grading. That variation in the sand grading had little effect for these high strength concrete but was observed to have a greater effect for lower strength concretes. For the lightweight aggregate high strength concrete D2 there was virtually no third or trailing zone. The characteristics of the curves of Fig. 8 are consistent with the failure surface characteristics described in the discussion of Fig. 6 and the bridging mechanisms described in the discussion of Fig. 7.

For fracture energy defined as the area under the curve of Fig. 7, analysis shows that for dense aggregate concretes quadrupling the compressive strength from 27.8 MPa to 111.6 MPa doubled the tensile strength but increased the fracture energy by only 41%. Further the fracture energy for that 111.6 MPa silica fume concrete was no better than the fracture energy measured by Jeang and Hawkins (1985) for a 62 MPa non -silica fume concrete. For the 78.6 MPa lightweight aggregate concrete the fracture energy was only 68% of the fracture energy of the 27.8 MPa dense aggregate concrete. When the fracture energy associated with aggregate bridging is defined as the area under the third segment of the curve of Fig. 7, then it is clear that the variations in energy are due primarily to variations in that area. Aggregate bridging provided 60% and 42% of the fracture energy of the 27.8 and 111.6 MPa dense aggregate concretes, respectively and only 11% of the energy for the 78.6 MPa lightweight aggregate concrete.

5 Concluding remarks

If fracture mechanics approaches are to be used in practice for quality control and design of concrete members, a fracture mechanics testing standard must be developed that can be used to derive characteristic CCS-COD relationships like those of Fig. 7 for different concretes. The tail of the relationship of Fig. 7 depends on the manner in which the crack extends through the concrete. That extension takes two forms of roughness, one related to the extent to which the crack passes through, rather than around, the large aggregate particles and the other related to the tortuosity of the crack through the depth of the specimen. These results show that in combination those two roughnesses determine the bridging energy associated with the tail of the CCS-COD relationship.

6 Acknowledgment

The studies reported in this paper were funded by the U.S. National Science Foundation under a grant to the University of Washington for the study of "Fracture Mechanics Applied to Concrete." MSM 831053.

7 References

Akutagawa, S. (1984) **Wedge Configuration and Loading History Considerations for Concrete CLWL-DCB Fracture Specimens,** MSCE Thesis, Dept. of Civil Engr., Univ. of Washington, Seattle.

Jeang, F.L. and Hawkins, N.M. (1985) **Non-Linear Analysis of Concrete Fracture,** Report SM 85-2, Dept. of Civil Engr., Univ. of Washington, Seattle.

Liaw, B.M., Jeang, F.L., Du, J.J., Hawkins, N.M. and Kobayashi, A.S. (1990) Improved non-linear model of concrete fracture. **J. of Engr. Mech., ASCE,** 116(2), 429-445.

Yin, X. (1997) **Concrete Fracture Process Zone Characteristics,** Ph.D. Thesis, Dept. of Civil Engr.., Univ. of Washington, Seattle.